Int. J. Heat Mass Transfer. Vol. 28, No. 8, pp. 1563–1574, 1985
Printed in Great Britain

0017–9310/85 $3.00 + 0.00
Pergamon Press Ltd.

Probes for local velocity and temperature measurements in liquid metal flow

THOMAS von WEISSENFLUH
Eidg. Technische Hochschule Zuerich, Institut fuer Reaktortechnik, CH-5303 Wuerenlingen, Switzerland

(*Received* 24 *September* 1984)

Abstract—A permanent magnet probe for local velocity, temperature and turbulent heat flux measurements in liquid metals is described. The sensitivity and the linearity of the probe are discussed and the thermoelectric and thermomagnetic sources of error are estimated, since they can be important. It is found that in flow regimes influenced by natural convection one has to correct for the thermoelectric effect. Results from isothermal and non-isothermal flow of liquid sodium at $Re = 40{,}000$ and $q_{wall} = 20.0\ \mathrm{kW\ m^{-2}}$ are presented and compared with previous data for liquid metals and air.

1. INTRODUCTION

THE MEASUREMENT of a turbulent velocity field in liquid metal flow is not a trivial matter. Widely used methods for velocity measurements in other fluids than liquid metals are not suitable for several reasons. Optical methods cannot be applied because of the opacity of liquid metals. Hot film sensors seem to be restricted to liquid mercury and do not work beyond fluid temperatures of 100°C [1–3]. Pitot tubes are troubled by the solidification of the liquid metal and only give values for the local mean velocity component [4, 5]. Since the application of semi-empirical turbulence models in liquid metal flows requires more information about the turbulent heat flux [6, 7], this is still an open field for development of measuring techniques.

A method for measuring velocity and temperatures simultaneously by a permanent magnet probe is described. The electromotive force induced in a liquid conductor (e.g. sodium) moving through a magnetic field is used. The electric potential is detected by two open-ended thermocouples, which are used to measure temperatures at the same time. A similar probe was described by Ricou and Vives [4], but this did not include temperature registration.

2. PRINCIPLE OF THE PROBE

The probe works on the basis of Faraday's law [8], i.e. if an electric conductor moves through a magnetic field the conductor has an electromotive force induced in it which is in a direction normal to the magnetic field and the direction of motion. It will be shown later, that the electromotive force generates an electric field which is nearly proportional to the intensity of the magnetic field and to the velocity of the conductor.

By miniaturizing the probe its influence on the hydrodynamic flow structure can be reduced. Also, by immersing the permanent magnet in the liquid metal, it is possible to reduce the magnetohydrodynamic effect on the flow to a minimum.

2.1. *Construction of the probes*

Since the measurements were made in a vertical circular duct, it was necessary to construct two different probes to measure all three velocity components. The axial probe [Fig. 1(a)] measures only the axial velocity component in the pipe, the radial probe [Fig. 1(b)] simultaneously measures the radial and azimuthal components. Both types of probe have a small cylindrical permanent magnet fabricated from a rare-earth element enclosed in the tip. The magnetic field is either transverse to the axis of the pipe, for measuring the axial velocity component, or parallel to the axis for measuring the transverse velocity components (radial and azimuthal). The two electrodes of two open-ended chromel–alumel thermocouples are used to measure

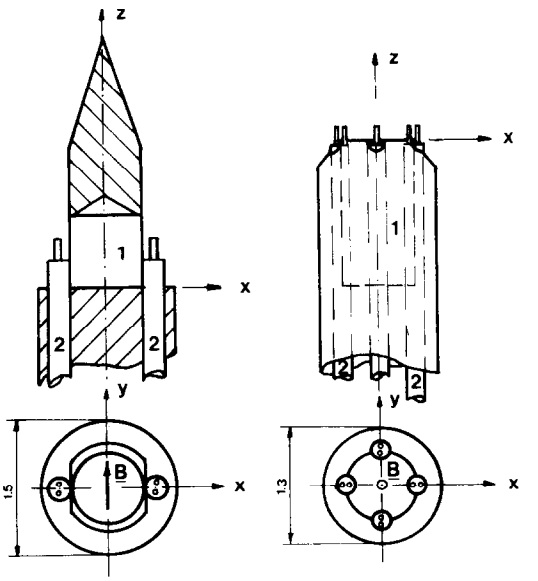

FIG. 1. (a) Axial velocity probe; (b) transverse velocity probe. (1) Rare-earth permanent magnet (RECOMA), (2) open-ended chromel–alumel thermocouple, **B** magnetic field direction.

NOMENCLATURE

A	specific work of flow, equation (15) [N m^{-1} s^{-1}]
$\mathbf{B}$	magnetic field [G]
B_0	strength of magnetic field on the surface of sphere [G]
C, C_a, C_c	inverse calibration factors, equations (23), (24) [m V^{-1} s^{-1}]
d	distance between thermocouples at the tip of the probe [m]
$\mathbf{E}$	induced electric field, equation (2) [V]
$\mathbf{E}'$	thermoelectric influences, equation (5) [V]
$E_x(f)$	auto-spectral density function
$E_{xy}(f)$	cross-spectral density function
$F_x(f)$	transfer function of amplifier/filter chain
G	Green's function [10]
$H_x(f)$	transfer function of probe signal $x(t)$
$\mathbf{j}$	electric current, equation (4) [A]
K	kinetic energy of flow, equation (17) [N m^{-1} s^{-1}]
L_0	characteristic length, equation (13) [m]
$\mathbf{n}$	vector normal to surface of sphere
Q	Ettinghausen–Nernst coefficient, equation (20) [V °C^{-1} G^{-1}]
R	radius of the magnetic sphere (Fig. 2) [m]
$R_{\overline{xy}}$	correlation coefficient of signals x and y
r	radius, cylindrical coordinate [m]
$\mathbf{r}', \mathbf{r}''$	points on the surface of the sphere (Fig. 2)
Re	Reynolds number, UD/ν
Re_m	magnetic Reynolds Number, equation (13)
S	thermoelectric coefficient [V °C^{-1}]
T	temperature [°C]
$\mathbf{U}, U_i$	velocity field, velocity component [m s^{-1}]
u_i	fluctuation of velocity component [m s^{-1}]
V, v	potential and potential fluctuation at electrodes [V]
$x(t), y(t)$	effective signals
$X(f), Y(f)$	Fourier transforms of effective signals
$z(t)$	measured signal
$Z(f)$	Fourier transform of measured signal.

Greek symbols

ΔT	temperature difference between the electrodes of a thermocouple [°C]
θ	temperature fluctuation [°C]
ϕ	cylindrical coordinate
μ	magnetic permeability ($4\P \times 10^{-7}$) [V s A^{-1} m^{-1}]
ρ	density of fluid [kg m^{-3}]
σ	electrical conductivity [Ω^{-1} m^{-1}]
Ω_0	vector of flow direction.

Subscripts

a	alumel thermocouple electrode
c	chromel thermocouple electrode
N	sodium
w	corrected by amplifier/filter transfer function.

Abbreviations

$\Delta V_a = V_{3a} - V_{4a}$
$\Delta V_c = V_{3c} - V_{4c}$
$\Delta v_1 = v_{3c} - v_{3a}$
$\Delta v_2 = v_{4c} - v_{4a}$
$\Delta v_a = v_{3a} - v_{4a}$
$\Delta v_c = v_{3c} - v_{4c}$.

the velocity-induced electric potentials. The thermocouples are similar to those developed by Bunschi *et al.* [9]. With these thermocouples it is possible to simultaneously measure fluctuations of temperatures and velocities with good spectral resolution. The turbulent heat flux can be determined from a cross-correlation of both signals—temperature and velocity fluctuations.

2.2. *Physical relations*

The induced potential can be defined by the stationary Maxwell equations (1)–(3) and Ohm's law (4):

$$\text{rot}\,\mathbf{B} = \mu\mathbf{j} \tag{1}$$

$$\text{rot}\,\mathbf{E} = 0, \quad \text{i.e.} \quad \mathbf{E} = -\text{grad}\,V \tag{2}$$

$$\text{div}\,\mathbf{B} = 0 \tag{3}$$

$$\mathbf{j} = \sigma(\mathbf{E} + \mathbf{E}' + \mathbf{U} \times \mathbf{B}). \tag{4}$$

In (4) the symbol $\mathbf{E}'$ stands for the thermoelectric and thermomagnetic influences. These are the two main disturbances affecting the induced electric potential.

$$\mathbf{E}' = -S\nabla T - Q(\nabla T \times \mathbf{B}). \tag{5}$$

Equations (1)–(5) lead to a Poisson equation for the potential V. The equation is tailored to the requirements of the probe, therefore only those effects

which influence the probe signal are considered

$$\nabla\cdot(\sigma\nabla V) = \nabla\cdot(\sigma\mathbf{U}\times\mathbf{B}) - \nabla\cdot(\sigma S\nabla T) - \nabla\cdot(\sigma Q(\nabla T\times\mathbf{B})). \quad (6)$$

From equation (6) we see that the velocity field **U**, the magnetic field **B** and the temperature T have an influence on the induced potential. The introduction of theoretical simplifications allows the performance of an idealized probe to be analysed.

2.3. *Sensitivity of the probe*

With a constant temperature field, T, equation (6) reduces to

$$\nabla\cdot(\sigma\nabla V) = \nabla\cdot(\sigma\mathbf{U}\times\mathbf{B}). \quad (7)$$

For the sake of simplicity a spherical permanent magnet is introduced instead of a cylindrical one. Superposition of a parallel and a dipole flow results in a potential flow around a sphere. The condition that the radial velocity component disappears on the surface of the sphere allows the strength of the source and sink of the dipole to be determined. Assuming that the field **B** is not disturbed by secondary currents [4], i.e. $\mathbf{j} = 0$ and therefore rot $\mathbf{B} = 0$, **B** is a potential field. Now with two potential fields, **B** and **U**, it is possible to modify equation (7). The RHS of (7) will disappear when σ is constant and the operation rule for vectors is followed:

$$\nabla\cdot(\mathbf{U}\times\mathbf{B}) = \mathbf{B}(\nabla\times\mathbf{U}) - \mathbf{U}(\nabla\times\mathbf{B}). \quad (8)$$

Since the velocity **U** is not a continuous function at the surface of the magnetic sphere, partial integration leaves one term on the LHS of equation (7). With continuity of the normal component of the electric current on the surface of the magnetic sphere we find for the potential V at any point $\mathbf{r}'$

$$V(\mathbf{r}') = \frac{1}{(\mathbf{r}')}\int_s G\sigma_N(\mathbf{U}\times\mathbf{B})\mathbf{n}\,\mathrm{d}s. \quad (9)$$

For potential flow around a sphere and with $\sigma_N = \sigma$ = constant, it is possible to integrate equation (9). Where G is Green's function on the surface of the sphere [10]. The potential flow around a sphere has the form [11]

$$\Psi = U_\infty\cdot\boldsymbol{\Omega}_0\cdot\mathbf{r} + \frac{Q}{r^3}\cdot\boldsymbol{\Omega}_0\cdot\mathbf{r}. \quad (10)$$

The components of the magnetic dipole are [12]

$$B_r = \frac{2p}{r^3}\sin\theta\cos\phi \quad (11a)$$

$$B_\theta = -\frac{p}{r^3}\cos\theta\cos\phi \quad (11b)$$

$$B_\phi = \frac{p}{r^3}\sin\phi. \quad (11c)$$

Integrating equation (9) with the components of **U** and **B** one can find an expression for the difference of the electric potential between any two points $\mathbf{r}'$ and $\mathbf{r}''$ when $B_0 = 2p/R^3$:

$$V(\mathbf{r}'') - V(\mathbf{r}') = \tfrac{1}{2}U_\infty B_0 R\sin\theta_0\sin\phi_0. \quad (12)$$

The potential difference in equation (12) depends on the angle of incidence of flow at the probe surface (Fig. 2) and on U_∞, B_0 and the radius of the spherical permanent magnet, R. If the main flow direction is normal to the direction of the magnetic field and also to the line between the two sensing elements, then $\sin\theta_0$ and $\sin\phi_0$ are both equal to unity. The theoretical sensitivity of the probe can be calculated to be 31.3×10^{-6} V s m^{-1}, with this geometrical configuration ($B_0 = 1000$ G). The probes give experimental values of about 30×10^{-6} V s m^{-1}. The good agreement between the two values is accidental, since the theoretical simplifications and assumptions for the calculations are very restrictive.

Equation (9) is valid for any velocity field and for any point around the spherical probe. It has been found [13] that the probe is sensitive to only one velocity component, if the electrodes are positioned exactly as shown in Fig. 2, i.e. symmetrical with respect to the centre of the volume and on an axis normal to the direction of magnetization. In addition, the probe output is a function of the cosine of the angle of incidence—a fact which was also found by Ricou and Vives [4, 13].

2.4. *Linearity of the probe*

When discussing the linearity of the probe, the influence of the magnetic field of the probe itself and the influence of the induced magnetic field on the velocity field have to be considered. The magnetic Reynolds number (Re_m) is defined by

$$Re_m = \mu\sigma L_0 U_0. \quad (13)$$

It represents the ratio of the induced field to the field of the magnet itself [12]. For $Re_m \ll 1$ the influence of the induced magnetic field can be disregarded.

The strength of the magnetic field of a spherical dipole decreases with the third power of the distance from the surface of the magnet [12]. At a distance of $5R$ from the surface, the field is weak enough not to disturb the turbulent structure of the flow. Taking this distance

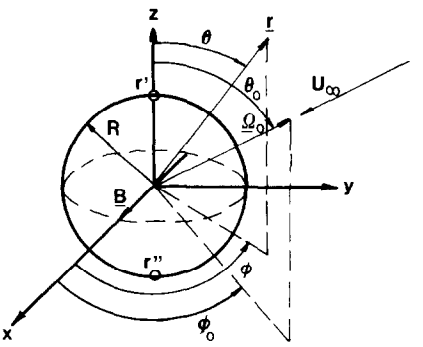

FIG. 2. Scheme of probe with spherical magnet.

as the radius of a sphere characterizing the area of influence of the magnet's field, the characteristic length L_0 in (13) is 12 times the radius of the magnetic sphere ($L_0 = 12R$). With $\mu = 4\P \times 10^{-7}$ V s A^{-1} m^{-1}, $\sigma = 7.5 \times 10^6$ Ω^{-1} m^{-1} and $U_0 = 1.0$ m s^{-1}, a magnetic Reynolds number $Re_m = 0.057$ is obtained. This means that the induced magnetic field can be neglected in the area where the field of the permanent magnet can have an influence on the turbulent flow structure. The same result was found in the dissertation of von Weissenfluh [13].

The induced current in the conducting liquid metal, together with the magnetic field, produce a force acting opposite to the direction of flow [8]. In the present case the specific work (N m^{-1} s^{-1}) as a function of distance from the surface of the magnet is compared with the kinetic energy of the flow. The induced electromagnetic force is proportional to the velocity and to the square of the magnetic field:

$$\mathbf{F} = \mathbf{j} \times \mathbf{B} = \sigma(\mathbf{E} \times \mathbf{B} + (\mathbf{U} \times \mathbf{B}) \times \mathbf{B}). \tag{14}$$

When evaluating the magnitude of **F** in equation (14), only the second term on the RHS has to be considered, as it is the largest term in the equation. The first term on the RHS is opposed to the second. Again considering a spherical permanent magnet the term $(\mathbf{U} \times \mathbf{B}) \times \mathbf{B}$ of (14) is approximated by the integral

$$A = \int_{-\P/2}^{+\P/2} \sigma U_\phi B_r B_r r \, d\phi. \tag{15}$$

The velocity direction is almost normal to the magnetic field all along the magnet, considering again a potential flow around a spherical probe. Equation (15) is therefore justified and can be evaluated for comparison with the kinetic energy (K) of the flow:

$$A = -\frac{4}{3}\sigma U \frac{B_0 R^6}{r^6}\left(1 + \frac{1}{2}\frac{R^3}{r^3}\right)r \tag{16}$$

$$K = (\rho_{Na}/2)U^2. \tag{17}$$

The values in the Table 1 have been calculated for the two mean velocity values of 1.0 m s^{-1} and 0.01 m s^{-1}, without considering a velocity reduction in the boundary layer. The ratio A/K is proportional to $1/U$, i.e. the smaller the velocity the higher the influence of the induced electromagnetic force. These results show that one has not to expect the probe to work linearly below velocities of 0.01 m s^{-1}. A velocity resolution of 0.01 m s^{-1} is set by the measuring equipment, this making it impossible to demonstrate the non-linearity of the probe experimentally.

Table 1. Relative influence on flow by the induced magnetic field

r/R	A/K $U = 1.0$ m s^{-1}	A/K $U = 0.01$ m s^{-1}
1.0	0.17	17
1.5	0.0167	1.67
2.0	0.0037	0.37
3.0	0.0005	0.05

2.5. *Thermal influences*

In an analogous procedure to that of Section 2.3, the velocity field **U** is now put to zero. The Poisson equation (6) then reduces to a temperature-dependent form:

$$\nabla \cdot (\sigma \nabla V) = -\nabla \cdot (\sigma S \nabla T + \sigma Q(\nabla T \times \mathbf{B})). \tag{18}$$

By the use of Green's function [10] it is possible to find the general solution of equation (18) [13]. It is clear that both thermal effects can be treated separately:

$$V(\mathbf{r}') = \frac{1}{\sigma(r')} \int_{\text{vol}} \sigma \nabla G(S \nabla T + Q(\nabla T \times \mathbf{B})) \, \text{dvol}. \tag{19}$$

Thermoelectric potential

The thermoelectric effect consists of the electrical potential difference between two points of an electrical conductor at two different temperatures. It is dependent on the temperature and on the material of the conductor. The thermoelectric potential is superimposed on the induced velocity potential and has to be eliminated to obtain proper velocity measurements. If the velocity measurements are made in areas without large temperature gradients the temperature dependence of the thermoelectric coefficient does not need to be considered, because of its small variation with temperature. The evaluation of equation (19) is not easy, but it is possible to make some simplifying assumptions about the temperature field. For a spherical magnet, a linear spatial temperature gradient and a thermoelectric coefficient S, equation (20) has been derived [13]:

$$V(\mathbf{r}'') - V(\mathbf{r}') = S(T(\mathbf{r}'') - T(\mathbf{r}')). \tag{20}$$

Thermomagnetic potential

In electrical conductors many different thermomagnetic effects can be present [15]. For this probe the main influence is due to the Ettinghausen–Nernst effect, which occurs in magnetic fields where there are large temperature gradients. With a temperature gradient in the y-direction, an equation similar to (20) is found if the two points with the potential sensing elements lie symmetrically about and opposite to the centre of the magnetic sphere and the line joining them is normal to the direction of the magnetic field [13] (see Fig. 2).

$$V(\mathbf{r}'') - V(\mathbf{r}') = Q \frac{\partial T}{\partial y} Bd. \tag{21}$$

Since the Ettinghausen–Nernst factor, Q, is much larger for permanent magnetic material than for sodium, the influence of the magnetic material on the velocity measurement is considered. The Q coefficients of the rare-earth elements are not known by the author, and so an estimate of the thermomagnetic effect has been made using the Q factor of nickel. For a temperature

gradient of 200°C m^{-1}, a magnetic field of $B = 4000$ G. Q(nickel, 35°C) $= 1.0 \times 10^{-10}$ V °C^{-1} G^{-1} and $d = 0.001$ m, a value of 0.08×10^{-6} V, is found for the Ettinghausen–Nernst effect. This potential difference is too small for it to be considered further.

2.6. *Potential equations*

From the discussion of the Poisson equation (18) it becomes obvious that it is not possible to calculate theoretically the potential difference between the two sensing points of the probe as a function of the velocity. It will be necessary to evaluate the calibration factors by experiment. Following the previous argument the potential difference for the present probe is the resultant of velocity and temperature components. Equation (22) is severely simplified since the general equations for the potential [equations (9) and (19)] show that it depends on the detailed definition of the velocity and temperature fields. In (22) only first-order effects are considered

$$V(\mathbf{r}'') - V(\mathbf{r}') = cUB_0R + S\Delta T. \tag{22}$$

Using the notation of Fig. 3 it is possible to develop the potential equations for the permanent magnet probe as follows:

$$V_{4a} - V_{3a} = S_a(T_1 - T_3) + S_a(T_4 - T_2) + S_N(T_2 - T_1) - C_aU_i \tag{23}$$

$$V_{4c} - V_{3c} = S_c(T_1 - T_3) + S_c(T_4 - T_2) + S_N(T_2 - T_1) - C_cU_i. \tag{24}$$

Assuming that the temperature differences between the two electrodes of each thermocouple are approx. zero:

$$\Delta T_1 \simeq \Delta T_2 \simeq 0. \tag{25}$$

The constants C_a and C_c in equations (23) and (24) become equal ($C_a = C_c = C$). With this simplification the calibration procedure reduces from two constants to a single value, C.

Velocity components

When both amplifier connectors are at the same temperature, $T_3 = T_4$, an equation for the velocity signal can be found from equations (23) and (24) (abbreviations are found in the nomenclature list):

$$CU_i = [(S_N - S_c)\Delta V_a - (S_N - S_a)\Delta V_c]/(S_a - S_c). \tag{26}$$

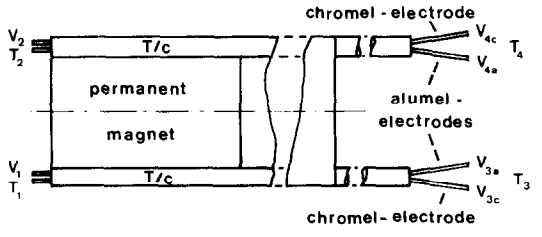

FIG. 3. Scheme of constructed probe with temperatures (T) and electrical potentials (V).

The constant C has the function of an inverse calibration factor in this equation and the method of determining C is described later. S_a and S_c, the thermoelectric coefficients of the alumel and chromel electrodes, are material constants. It is possible to calculate an equation for the mean square value of the velocity fluctuations, splitting the variable quantity into a mean and a fluctuation component ($\tilde{V} = V + v$):

$$C^2\overline{u_i^2} = [\overline{\Delta v_c^2}(S_N - S_a)^2 - 2\overline{\Delta v_c \Delta v_a}(S_N - S_a) \times (S_N - S_c) + \overline{\Delta v_a^2}(S_N - S_c)^2]/[(S_a - S_c)^2]. \tag{27}$$

Temperature

The mean temperature signal can be found, using the simplification of equation (25)

$$T_3 - T_1 = (V_{3c} - V_{3a})/(S_c - S_a) \tag{28}$$

$$T_4 - T_2 = (V_{4c} - V_{4a})/(S_c - S_a). \tag{29}$$

Since $T_3 = T_4 =$ constant, equations (28) and (29) are also valid for temperature fluctuations [13].

Turbulent heat flux

The correlation function of the velocity and temperature fluctuations, $\overline{u_i\theta}$, is called turbulent heat flux. Its equation is calculated from the potential equations (23), (24) and (28), (29):

$$\overline{Cu_i\theta_1} = \frac{\overline{\Delta v_1 \Delta v_a}}{(S_a - S_c)} - (\overline{\Delta v_1^2} - \overline{\Delta v_1 \Delta v_2}) \frac{S_N - S_a}{(S_a - S_c)^2} \tag{30}$$

$$\overline{Cu_i\theta_2} = \frac{\overline{\Delta v_2 \Delta v_a}}{(S_a - S_c)} - (\overline{\Delta v_1 \Delta v_2} - \overline{\Delta v_2^2}) \frac{S_N - S_a}{(S_a - S_c)^2}. \tag{31}$$

3. CORRECTIONS AND CALIBRATIONS

In equations (26), (27) and (30), (31) the velocity signal has been corrected for the influence of a possible temperature difference at the probe tip. This difference occurs only in non-isothermal flows (i.e. unheated or uncooled). To compensate for this effect it is necessary to measure two potential differences simultaneously for the velocity fluctuations (Δv_a, Δv_c) and three for the heat flux components (Δv_a, Δv_1, Δv_2).

The presence of the probe itself influences the thermoelectric potential difference between the two electrodes in contact with the sodium (19). Consequently, the thermoelectric coefficient which should be used is not exactly that of pure sodium. The real value S_N^* has to be determined experimentally from the difference between the probe signals for unheated (isothermal, i) and heated (non-isothermal, ni) flows at equal velocity:

$$S_N^* = \frac{S_c[(\Delta V_a)_{ni} - (\Delta V_a)_i] - S_a[(\Delta V_c)_{ni} - (\Delta V_c)_i]}{[(\Delta V_a)_{ni} - (\Delta V_a)_i] - [(\Delta V_c)_{ni} + (\Delta V_c)_i]}. \tag{32}$$

It is also possible to determine the value of S_N^* from the velocity fluctuations [13]. The important feature of these measurements is that the temperature is a passive scalar. This means that the temperature differences

have to be small enough not to influence the velocity distribution through natural convection.

3.1. *Dynamic corrections*

Dynamic corrections are associated with the spectral distribution of the measured fluctuations of velocities and temperatures. The four main reasons for these corrections are:

(a) The fluctuations of the turbulent flow are disturbed by the physical presence of the probe.

(b) The induced electromagnetic force acting opposite to the direction of flow reduces the magnitude and frequency of the turbulent velocity fluctuations around the probe, due to damping.

(c) The probe measures averaged velocity and temperature over a small volume of liquid metal, instead of point values.

(d) Finally the transfer function of the probe itself, including inertia effects, influences the results.

After having corrected for the transfer function of the amplifier/filter chain, the influences (a)–(d) are combined in one function, $H(f)$. The same general procedure is valid for both velocity and temperature measurements. Letting $Z(f)$ be the Fourier transform of the measured signal $z(t)$ and $X(f)$ be the Fourier transform of the effective signal $x(t)$, the following equation is valid [16]:

$$Z(f) = F(f)H(f)X(f) \tag{33}$$

$F(f)$ is the transfer function of the amplifier/filter chain and $H(f)$ is the transfer function of the probe. The auto-spectral density (ASD) function is then [16]

$$E_z(f) = |H(f)|^2|F(f)|^2E_x(f). \tag{34}$$

$F(f)$ is known from the data sheets of the manufacturers of the amplifiers and filters. It is computed at each data point. $H(f)$ is obtained from the comparison of experimental data and other spectral measurements. These measurements are the best which can be found in the literature of turbulent structure research. Adopting this procedure it is possible to modify the present measurements by using the results from methods with better spectral resolution [13, 17].

It is possible to obtain a simple solution for the correction function $H(f)$ to a first-order approximation, after the measured signals have been corrected by $F(f)$ and the modifying procedure above has been introduced:

$$\int_0^\infty \frac{E_z(f)}{\overline{z^2}}\,\mathrm{d}f = 1 \quad \text{and} \quad \int_0^\infty \frac{E_x(f)}{\overline{x^2}}\,\mathrm{d}f = 1 \tag{35}$$

$$E_w(f) \equiv \frac{E_z(f)}{|F(f)|^2} = |H(f)|^2E_x(f) \tag{36}$$

$$\int_0^\infty \frac{E_w(f)}{|H(f)|^2\overline{w^2}}\,\mathrm{d}f = \frac{\overline{x^2}}{\overline{w^2}}\int_0^\infty \frac{E_x(f)}{\overline{x^2}}\,\mathrm{d}f = P^2(f) \tag{37}$$

$$|H(f)|^2 = \frac{\overline{w^2}}{\overline{x^2}}\,\frac{E_w(f)/\overline{w^2}}{E_x(f)/\overline{x^2}}. \tag{38}$$

Assuming that for small frequencies $|H(f)|^2 = 1$,

$$\frac{E_w(f)/\overline{w^2}}{E_x(f)/\overline{x^2}} = \frac{\overline{x^2}}{\overline{w^2}} = P^2. \tag{39}$$

In equations (36)–(39) $\overline{w^2}$ is the mean square value of the measured signal corrected by the transfer function of the amplifier/filter chain (36). The dimensionless wavenumber (kD) is introduced when calculating the value of P^2. In dimensionless wavenumber form the spectral distributions of velocity fluctuation measurements in different fluids can be compared [18]. A constant, P, will be included in the calibration factor.

The product of the probe transfer functions for the velocity $H_x(f)$ and the temperature $H_y(f)$ appears in the equation for the cross-spectral density (CSD) function of the turbulent heat flux $\overline{u_i\theta}$:

$$E_{xy}^{\text{out}}f) = H_x^*(f)F_x^*(f)H_y(f)F_y(f)E_{xy}^{\text{in}}(f). \tag{40}$$

$H_x^*(f)$ and $F_x^*(f)$ are the conjugate complex transfer functions of the velocity signals and the corresponding amplifier/filter chain. The full form of the correlation coefficient is defined as

$$R_{\overline{xy}} = \int_0^\infty \frac{E_{xy}(f)}{H_x^*(f)F_x^*(f)H_y(f)F_y(f)}\,\mathrm{d}f \times \left(\int_0^\infty \frac{E_{xw}(f)}{|H_x(f)|^2}\,\mathrm{d}f\right)^{-1/2}\left(\int_0^\infty \frac{E_{yw}(f)}{|H_y(f)|^2}\,\mathrm{d}f\right)^{-1/2}. \tag{41}$$

The transfer functions of the amplifier/filter chain for velocity and temperature signals are approximately equal. The transfer function of a low noise signal transformer (Fig. 4) is dependent on the input impedance. These impedances are not too different for the velocity and the temperature probes. The product $F_x^*(f)F_y(f)$ is then approximately real. The transfer function of the velocity signal of the probe, is real because the damping of the signal is a result of volume averaging and not of inertia effects [4]. The transfer function of the temperature signal is likewise assumed to be real at lower frequencies. The energy part of the CSD-distribution lies below 1 in a dimensionless wavenumber representation [17, 18]. The important

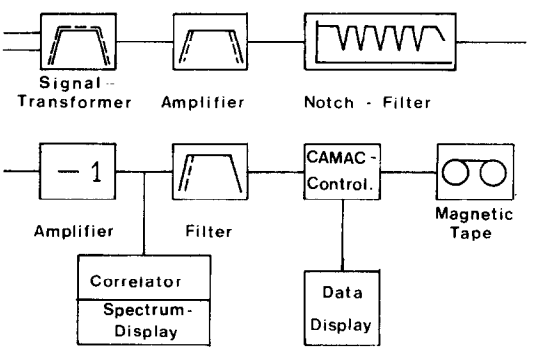

FIG. 4. Filter/amplifier chain for recording fluctuation signals.

temperature fluctuations for the correlation originate at frequencies below 10 Hz. Equation (41) reduces to

$$R_{\overline{u_i\theta}} = \frac{(\overline{u_i\theta})_w}{(\overline{u_i^2}\,\overline{\theta^2})_w^{1/2}}. \quad (42)$$

3.2. *Calibration*

As mentioned earlier the experimental calibration of a probe is necessary, in order to include the effects of other influences not yet considered. These are, for example, the exact form of the magnetic field, the contact resistance between sodium and the electrodes and losses by electric conduction at the tip of the probe.

Velocity calibration can be performed in different ways.

(a) The axial velocity probe is positioned at the centre of a pipe. The voltage output of the velocity signal is then measured at different Reynolds numbers in isothermal flow. There is no velocity or temperature gradient to influence the measurements in such a procedure. The Reynolds number is normally related to a bulk velocity. Thus the velocity U_{max} is measured in the centre of the pipe with the ratio U_{bulk}/U_{max} being a function of Re [5].

(b) The profile in the pipe is measured with an axial velocity probe. Integrating the profile and comparing it with the flow rate will give the calibration factor.

(c) The third procedure is not an absolute calibration method. It consists in comparing the measured velocity fluctuations with measurements in other fluids and with the results of other methods to give a calibration factor. Since the probes should work linearly down to velocities of a few cm s^{-1}, approximately the same calibration factor should result as in the other two cases. This method enables one to calibrate the transverse probe without having a mean transverse velocity component.

The temperature calibration is not discussed here, because it is based on the well-known technology of thermocouples.

4. RESULTS

4.1. *Test section and measuring equipment*

The measurements were carried out in a small sodium test-loop (with 42 dm^3 of sodium) which had previously been used by Fuchs [5] and Bunschi [19]. The test section was of circular cross section with an inner diameter of $D = 0.0030$ m, a total length of 1.80 m ($60D$) and a heated length of 1.44 m ($48D$). The liquid sodium flowed upwards in the vertical test-section and the two probes were inserted from the top, through a positioning head [13].

Different measurement and recording equipments were used for the mean and fluctuating components of the velocity and temperature signals. The mean values were measured by a Keithley nanovoltmeter (M 148) and a two channel paper-tape recorder. The fluctuation data were processed record-by-record by a CAMAC controller before they were written to magnetic tape (4096 words/record). The maximum sampling rate was 1000 s^{-1}. The amplifier/filter chain for the velocity and temperature fluctuation signals is shown in Fig. 4.

4.2. *Calibration*

All three calibration methods of Section 3.2 were applied to the data obtained from the probes. The results are listed in Table 2. The two calibration procedures for the mean values of the axial probe show good agreement. The difference between profile integration and the fluctuation calibration method is due to damping and to large differences in the velocity fluctuation data given in the literature, which are used by the method.

4.3. *Velocity and temperature profiles*

Figure 5 shows the turbulent velocity profiles in sodium pipe flow at $Re = 40{,}000$. For comparison the theoretical velocity profile of Reichardt [20] is shown with the measured profiles of isothermal and heated ($Q_{wall} = 20.0\,kW\,m^{-2}$) sodium pipe flow. The deviation from the theoretical profile is less than 5% for $r/R < 0.8$. The largest difference is found near the wall. This is consistent with the assumptions in the theoretical model for the influence of the flow field around the probe. In the neighbourhood of the wall, the flow surrounding the probe is severely disturbed and, in addition the volume of integration is reduced. The velocity profiles of Eyler [18] and Hochreiter [21] in mercury agree very closely with theory. The agreement between the measured velocity profile for heated and isothermal flow is good, when correction is made for the influence of temperature.

Table 2. Calibration factors

Method	Calibration factor $\times 10^{-4}$ V s m^{-1}	Re
Axial probe		
$f(Re)$	0.35 ± 0.01	0 to 80×10^3
Integration of profile	0.34	40×10^3
Integration of profile	0.35	80×10^3
Fluctuations	0.31	40 and 80×10^3
Transverse probe		
Fluctuations	0.28	40 and 80×10^3

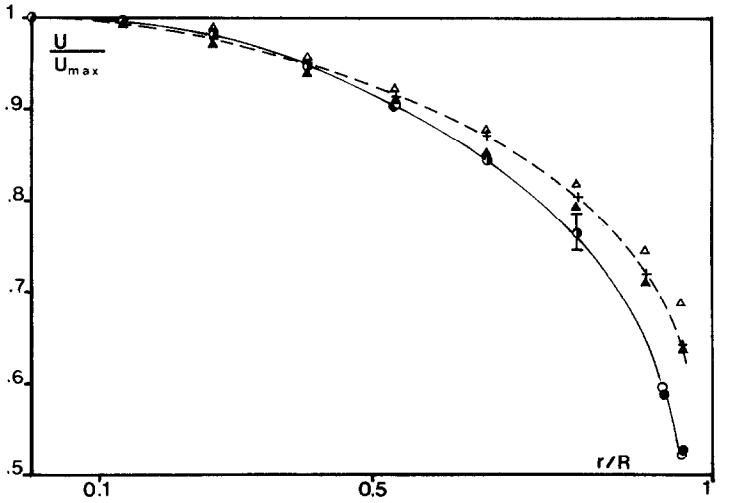

FIG. 5. Velocity profiles in pipe. △ [18], mercury, $Re = 50{,}000$; ▲ [21], mercury, $Re = 50{,}000$; + [20], theoretical $Re = 40{,}000$; ○ present data, sodium, $Re = 40{,}000$, isothermal; ● present data, sodium $Re = 40{,}000$, heated $q_{wall} = 20.0\ \text{kW m}^{-2}$.

The temperature profile is compared with the results of Fuchs [5] in Fig. 6. It is possible to eliminate the dependence of temperature profile on wall heat flux by normalizing the local temperature difference $(T - T_0)$ relative to the temperature difference between pipe wall and centre $(T_w - T_0)$. The agreement between the temperature profiles of Fuchs and the present data is within experimental accuracy.

4.4. *Velocity fluctuations*

Figures 7 and 8 show the fluctuation profiles of the axial and radial velocity components measured in the pipe. Since the data for the velocity fluctuations given in the literature differ by $\pm 20\%$ [18, 21–25] the measured profiles show large differences when compared with data from the literature.

The axial velocity fluctuations are shown in Fig. 7. The present data have higher values than the measurements in air [22] and mercury [21, 23, 24] in the region $0.5 < r/R < 0.8$. Values at the pipe centre are the same because the calibration was based on agreement at this point. For $r/R > 0.8$ the present data decrease, although the other measurements show increasing values up to $r/R = 0.9$. The reason for this characteristic deviation is the nearness of the wall, influencing the output of the potential probe.

Figure 8 shows the profile of radial velocity fluctuations. The present data are in close agreement with those given for comparison. For $0.8 < r/R < 0.95$ the data found in the literature are contradictory [18, 22]. The present data show a decrease for $r/R > 0.8$ which is due to the proximity of the wall.

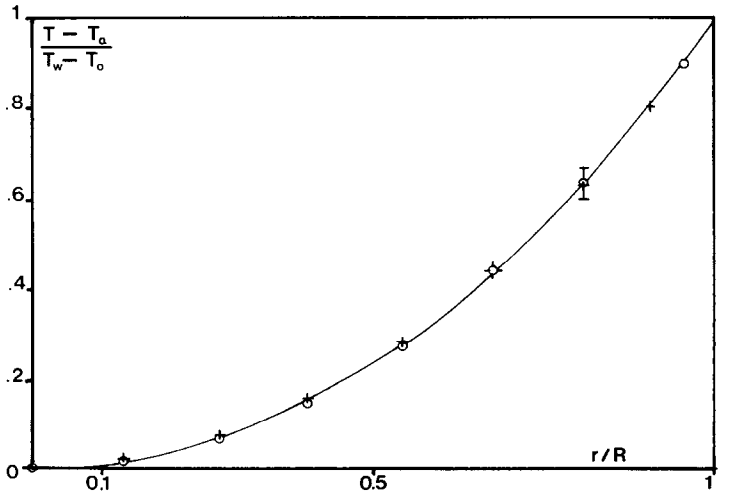

FIG. 6. Temperature profiles in pipe. + [5], $Re = 40{,}000$; ○ present data, $Re = 40{,}000$.

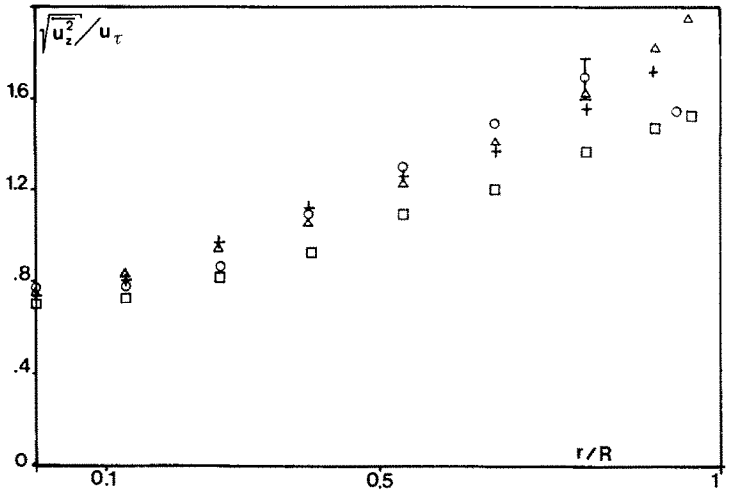

FIG. 7. Axial velocity fluctuations. △ [18], mercury, $Re = 50{,}000$; □ [22], air, $Re = 35{,}000$. + [25], air, $Re = 50{,}000$; ○ present data, $Re = 40{,}000$.

The azimuthal velocity component and the temperature fluctuations are not shown for the reason of limited space. The corresponding spectral distributions of the temperature and all the velocity fluctuation components are presented and discussed in the dissertation of von Weissenfluh [13].

4.5. *Turbulent heat flux*

The correlation coefficient of the axial turbulent heat flux is shown in Fig. 9. The results of Bremhorst and Bullock [23] for air, and Eyler's measurements in mercury [18], are also shown for comparison. The data of Eyler agree with the magnitude of the values of the present data but not with the shape of the radial distribution. The correlation coefficient for air appears to be higher than for sodium. Hochreiter's data [21] are omitted since they lead to a coefficient with values up to three and with negative sign.

The correlation coefficient for the radial turbulent heat flux is shown in Fig. 10. For constant wall heat flux and variable Reynolds Number different distributions of the coefficient are found for $r/R < 0.4$ and $r/R > 0.4$. With higher Re (80,000) the value of $R_{\overline{u_r\theta}}$ decreases towards the centre of the pipe ($r/R < 0.4$), while in the outer part of the pipe ($r/R > 0.4$) the correlation coefficient increases, compared with the values for $Re = 40{,}000$. The radial correlation coefficient calculated from the data of Fuchs [5] and Bunschi [19] decreases with increasing velocity over the whole pipe radius. The measurements in air taken by Ibragimov [26] show decreasing $R_{\overline{u_r\theta}}$ and $R_{\overline{u_z\theta}}$ with increasing Re at all radial positions in a pipe.

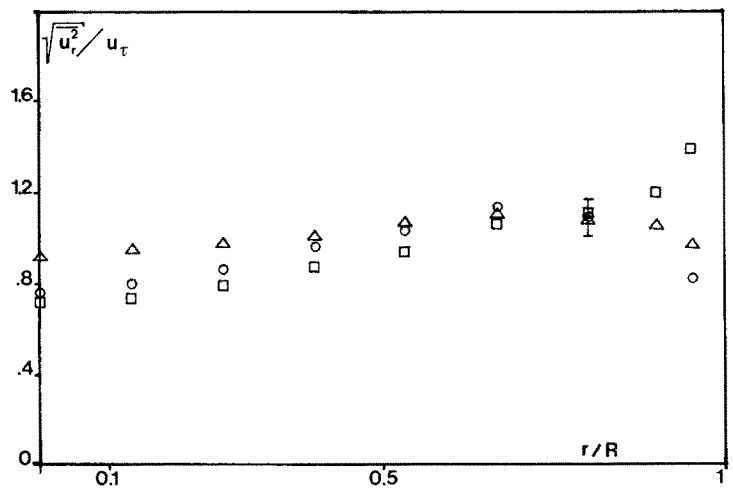

FIG. 8. Radial velocity fluctuations (symbols as Fig. 7).

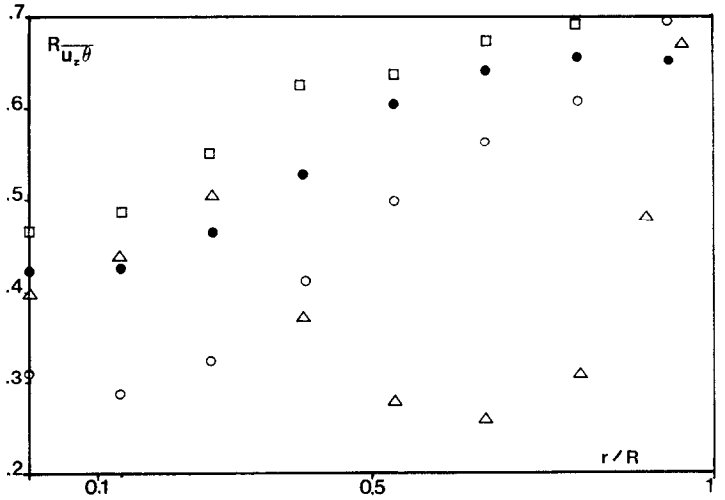

FIG. 9. Correlation coefficient for axial turbulent heat flux. + [5, 19], sodium, $Re = 40{,}000$; × [5, 19], sodium, $Re = 60{,}000$; △ [18], mercury, $Re = 50{,}000$; □ [23], air, $Re = 34{,}700$; ▼ [26], air, $Re = 32{,}500$; ○ present data, sodium, $Re = 40{,}000$; ● present data, sodium, $Re = 80{,}000$.

5. CONCLUSIONS

When the characteristic dimensions of the flow geometry are much larger than those of the probe, the results obtained with the potential probe are of acceptable accuracy, though the spatial and spectral resolutions of hot-film anemometers have not been achieved. However, this appears to be a valuable method of obtaining information from turbulent liquid metal flows. If natural convection has an influence on the velocity distribution it is important to make correction for the temperature difference between the two sensing points of a magnetic potential probe. Nevertheless the probe produces reliable results only if the spatial temperature distribution is approximately linear in the vicinity of the probe.

Deeper understanding is needed of the physical effects that determine the frequency dependence of the probe transfer functions, in order that probe calibration can be improved. Probe size has to be increased if it is required to use a permanent magnet material that can resist higher ambient temperature without damage. In this case it is possible to obtain the same velocity resolution but the frequency resolution is reduced. Thermocouples with three electrodes, two for the temperature measurements and one for the velocity component connected to the shielding of the thermocouple showed less sensitivity to frequency. Therefore a probe constructed to operate at higher ambient temperature did not deliver results of the same quality as those produced by the rare-earth element permanent magnets with open-ended thermocouples.

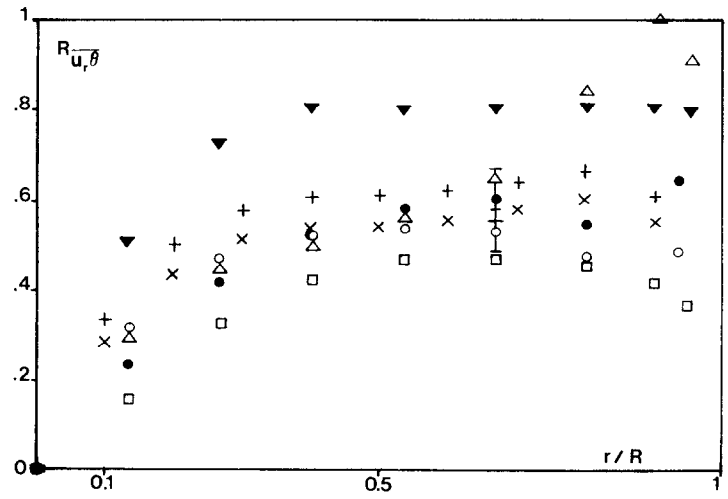

FIG. 10. Correlation coefficient for radial turbulent heat flux (symbols as Fig. 9).

Acknowledgement—The author gratefully acknowledges the help of Dr B. Sigg in all parts of the work as well as the support of Professor W. Haelg. Special thanks is due to T. V. Dury for his careful review of the English version.

REFERENCES

1. R. J. Holroyd, Hot film probe measurements in liquid metal MHD duct flow experiments, *DISA Inf.* **25**, 19–25 (1980).
2. D. G. Malcolm, Some aspects of turbulence measurements in liquid mercury using cylindrical quartz insulated hot-film sensors, *J. Fluid Mech.* **37**, 701–713 (1969).
3. I. A. Platnieks, Comparison of the hot-wire anemometry and conduction methods for mercury measurements, *Gidrod.* **7**, 140–142 (1971).
4. R. Ricou and C. Vives, Local velocity and mass transfer measurement in molten metals using an incorporated magnet probe, *Int. J. Heat Mass Transfer* **25**, 1579–1588 (1982).
5. H. Fuchs, Waermeuebergang an stroemendes Natrium. Ph.D. thesis ETH Zuerich, Switzerland, Nr. 5110 (1972).
6. B. E. Launder, Heat and mass transport. In *Turbulence* (edited by P. Bradshaw), 2nd edn, *Topics in applied Physics* Vol. 12, pp. 232–287 (1978).
7. W. C. Reynolds and T. Cebeci, Calculation of turbulent flows. In *Turbulence* (edited by P. Bradshaw), 2nd edn. *Topics in applied Physics* Vol. 12, pp. 193–229 (1978).
8. J. A. Shercliff, *The Theory of Electromagnetic Flow Measurement*. Cambridge University Press, Cambridge (1966).
9. H. Bunschi and W. Seifritz, A fast response thermocouple for temperature fluctuation measurements in sodium coolants, *Ann. Nucl. Energy* **2**, 415–417 (1975).
10. J. Irving and M. Mullineux, *Mathematics in Physics and Engineering*. Academic Press, New York (1959).
11. H. H. Thomann, Stroemungslehre II, ETH Zuerich, Switzerland (1970).
12. E. Kneller, *Ferromagnetismus*. Springer, Berlin (1962).
13. T. von Weissenfluh, Turbulenter Waermetransport in fluessigem Natrium. Ph.D. thesis, ETH Zuerich, Switzerland, Nr. 7464 (1984).
14. J. M. Rosant, Ecoulements hydromagnetiques turbulents en conduite rectangulaire. Thèse doct. ing., University of Grenoble (1976).
15. T. G. Kollie, T. H. Anderson, J. L. Horton and M. J. Roberts, Large errors in thermocouple thermometry, *Rev. Scient. Instrum.* **48**, 5–17 (1977).
16. J. S. Bendat and A. G. Piersol, *Measurement and Analysis of Random Data*. John Wiley, New York (1966).
17. T. von Weissenfluh and B. Sigg, Probes for local velocity and heat flux measurements in liquid metals, XV ICHMT, Symposium on Heat and Mass Transfer Measurement Techniques, Dubrovnik (1983).
18. L. L. Eyler, Turbulent structure measurement and thermal transport modeling in liquid metals. Ph.D. thesis, Purdue University (1978).
19. H. Bunschi, Turbulente Temperaturschwankungen in fluessigem Natrium. Ph.D. thesis, ETH Zuerich, Switzerland, Nr. 5890 (1977).
20. H. Reichardt, Vollstaendige Darstellung der turbulenten Geschwindigkeitsverteilung in glatten Leitungen, *Z. angew. Math. Mech.* **31**, 208–219 (1951).
21. L. Hochreiter, Turbulent structure of isothermal and non-isothermal liquid metal pipe flow. Ph.D. thesis, Purdue University (1971).
22. K. Bremhorst and K. J. Bullock, Spectral measurement of temperature and longitudinal velocity fluctuations in fully developed pipe flow, *Int. J. Heat Mass Transfer* **13**, 1313–1329 (1970).
23. K. Bremhorst and K. J. Bullock, Spectral measurement of turbulent heat and momentum transfer in fully developed pipe flow, *Int. J. Heat Mass Transfer* **16**, 2141–2154 (1973).
24. C. J. Lawn, The determination of the rate of dissipation in turbulent pipe flow, *J. Fluid Mech.* **48**, 447–505 (1971).
25. J. Laufer, The structure of turbulence in fully developed pipe flow, Nat. Bureau of Stand., Report Nr. 1174 (1954).
26. M. K. Ibragimov, V. I. Subbotin and F. S. Taranov, Korrelation von Geschwindigkeits und Temperaturschwankungen in stroemender Luft, *Int. chem. Engng* **11**, 659–666 (1971).

SONDES POUR LES MESURES LOCALES DE VITESSE ET DE TEMPERATURE DANS UN ECOULEMENT DE METAL LIQUIDE

Résumé—Une sonde à aimant permanent est décrite pour les mesures locales de vitesse, de température et de flux de chaleur par turbulence dans les métaux liquides. La sensibilité et la linéarité de la sonde sont discutées et les sources d'erreur thermoélectriques et thermomagnétiques sont estimées, car elles peuvent être importantes. On trouve que dans les régimes d'écoulement influencés par la convection naturelle, on doit corriger pour l'effet thermoélectrique. Des résultats sur l'écoulement de sodium liquide isotherme ou non-isotherme, à $Re = 40\,000$ et q (paroi) = 20 kW m^{-2}, sont présentés et comparés avec des données antérieures pour les métaux liquides et l'air.

SONDEN FÜR LOKALE GESCHWINDIGKEITS- UND TEMPERATURMESSUNGEN IN STRÖMUNGEN VON FLÜSSIGEN METALLEN

Zusammenfassung—Es wird eine Permanent-Magnetsonde für lokale Geschwindigkeits-, Temperatur- und turbulente Wärmestrommessungen in flüssigen Metallen beschreiben. Die Empfindlichkeit und die Linearität der Sonde werden diskutiert und die thermoelektrischen und thermomagnetischen Fehlerquellen, da sie wichtig sein können, abgeschätzt. Es stellt sich heraus, daß bei Strömungen, die durch natürliche Konvektion beeinflußt werden, eine Korrektur aufgrund des thermoelektrischen Effekts notwendig wird. Ergebnisse für isotherme und nicht-isotherme Strömung von flüssigem Natrium bei $Re = 40000$ und q(Wand) = 20,0 kW m^{-2} werden vorgestellt und mit früheren Daten für flüssige Metalle und Luft verglichen.

ДАТЧИКИ ДЛЯ ИЗМЕРЕНИЯ ЛОКАЛЬНЫХ СКОРОСТЕЙ И ТЕМПЕРАТУР В ПОТОКЕ ЖИДКОГО МЕТАЛЛА

Аннотация—Описывается стационарный магнитный датчик для измерения локальных скоростей, температур и турбулентных тепловых потоков в жидких металлах. Обсуждаются чувствительность датчика и линейность его характеристик, а также оцениваются термоэлектрические и термомагнитные источники ошибок. Найдено, что при режимах течения на которые оказывает влияние свободная конвекция, необходимо учитывать термоэлектрический эффект. Представленные результаты для изотермического и неизотермического режимов течения жидкого натрия при $Re = 40000$ и, q (стенки) = 20,0 кВт/м^2 сравниваются с данными, полученными ранее для жидких металлов и воздуха.